Coarse bedload routing and dispersion through tributary confluences

Kurt S. Imhoff[1*], Andrew C. Wilcox[1]

[1] Department of Geosciences, 32 Campus Drive #1296, University of Montana, Missoula, MT 59812

Correspondence to: kurt.imhoff@umontana.edu

Abstract

Sediment routing fundamentally influences channel morphology and propagation of disturbances such as debris flows. The transport and storage of bedload particles across headwater channel confluences, which may be significant nodes of the channel network in terms of sediment routing, morphology, and habitat, are poorly understood, however. We investigated patterns and processes of sediment routing through headwater confluences by comparing them to published results from lower-gradient confluences and by comparing the dispersive behavior of coarse bedload particles between headwater confluence and non-confluence reaches. We addressed these questions with a field tracer experiment using passive-integrated transponder and radio-frequency identification technology in the East Fork Bitterroot River basin, Montana, USA. Within the confluence zone, transport occurred along scour-hole margins in narrow, efficient transport corridors that mirror those observed in prior studies, many of which are from finer-grained systems. Coarse particles entering confluences experienced reduced depositional probabilities relative to a control reach. Analysis of the distribution of particle transport lengths suggested that variation in the spatial distribution of coarse sediment particles was enhanced by passing through confluences. We suggest that equilibrium confluences can enhance sediment transport through headwater networks.

1 Introduction

The transport and storage of mobile sediment particles through channel networks, i.e., sediment routing (Swanson and Fredriksen, 1982), link sediment supply, flow, and channel morphology and thereby regulate channel evolution (Church, 2002; Church 2006). In headwater regions, where hillslope-channel connectivity is strong, storage and downstream routing of sediment inputs reflect the influence of spatially and temporally variable forcing by hillslope (e.g., debris flows) and fluvial processes (Montgomery and Buffington, 1997; Brooks and Brierley, 1997; Prosser et al., 2001; Lancaster and Casebeer, 2007). Discrete pulses of coarse sediment delivered to streams can travel downstream as a translating bedload wave, by dispersion, or by a combination of translation and dispersion (Lisle et al., 2001; Sklar et al., 2009).

Analyses of dispersion based on the premise that particle motion is a random walk have represented downstream transport as a series of intermittent steps and rests (Einstein, 1937). This approach has informed flume and field studies seeking to identify characteristic probability distributions of step length and rest periods (e.g., Hubbell and Sayre, 1964; Yang and Sayre, 1971; Bradley et al., 2010). Statistical distributions, including exponential, gamma, and Pareto functions, have been found to approximate spatial distributions of bedload-particle displacements in flume and field conditions (e.g., Hassan et al., 1991; Bradley and Tucker, 2012; Martin et al., 2012; Haschenburger, 2013, Phillips et al., 2013). These statistical models have been used to approximate dispersive regimes in various gravel-bed channel morphologies, including plane-bed (Bradley and Tucker, 2012), pool-riffle (Liébault et al., 2012; Milan, 2013), and braided systems (Kasprak et al., 2014). Many model functions may be applicable, however, because morphologic features and hydraulics can produce characteristic local dispersive regimes (Pyrce and Ashmore, 2003). Long-term tracer experiments have noted evolving spatial distributions of bedload particles, suggesting that best-fit statistical distributions may differ depending on the degree of vertical mixing, often a function of time (Haschenburger, 2013). As a result, dispersion models predicting a smooth spatial distribution may not adequately capture the true dispersive behavior of bedload particles across multiple channel morphologies.

The dispersive behavior of coarse sediment particles has also been considered in terms of changes in the variance of particle displacements with time (e.g., Phillips et al., 2013). Sediment dispersion is thus treated as analogous to one-dimensional diffusion in the downstream direction, with potential diffusion dynamics that include normal diffusion, where the variance of particle displacements increases linearly with time, and anomalous diffusion, which includes both superdiffusion and subdiffusion, when variance increases more quickly or more slowly with time than the linear case, respectively (Metzler and Klafter, 2000; Nikora et al., 2002; Olinde and Johnson, 2015). Improved understanding of variability in dispersive regimes among channel types and other controls on sediment dispersion is needed, however, to facilitate sediment-routing predictions.

Nodes of the channel network that may be especially important with respect to sediment routing are tributary confluences, where point sources of flow and sediment connect tributary to trunk streams. The importance of confluences in sediment routing, as well as their morphologic significance, may depend on factors including drainage densities (i.e., frequency of confluences; Benda et al., 2004), the magnitude and frequency of disturbances such as debris flows (Benda and Dunne, 1997; Hoffman and Gabet, 2007), and the relative differences in flow, sediment caliber, and load between tributaries and the trunk streams they enter (Figure 1) (Knighton, 1980; Richards, 1980, Ferguson et al., 2006, Swanson and Meyer, 2014). Morphological effects stemming from disturbance-derived confluence deposits may extend spatially, well beyond the area of flow convergence, and temporally, persisting for ~10^2 – 10^4 years (Lancaster and Casebeer, 2007). Study of confluences in light of disturbance deposits and morphological heterogeneity has led to the Network Variance Model (NVM, Benda et al., 2004), which considers the spatial arrangement of confluences in river networks and how they affect local and non-local channel morphological characteristics. Channel confluences also represent biological "hot spots", forcing spatial heterogeneity in habitat types and in various habitat metrics and influencing longitudinal distributions of aquatic organisms (Rice et al., 2001; Gomi et al., 2002).

Whereas sediment dynamics and morphology of headwater confluences can be primarily influenced by disturbances such as debris flows (Benda and Dunne, 1997), what we refer to as "equilibrium" confluence morphology, reflecting feedbacks between flow hydraulics, sediment

transport, and morphology, can also develop and persist (Figure 1). Such confluences are well-studied in sand and gravel-bed river systems and typically feature a central scour hole, tributary-mouth bars, and bank-attached bars at areas of flow recirculation and stagnation (Best, 1987; Rhoads, 1987; Best, 1988; Roy and Bergeron, 1990; Biron et al., 1996; Boyer, 2006; Rhoads et al., 2009; Ribeiro et al., 2012). Physical controls on confluence hydraulics and associated morphology include junction angle (Θ), bed discordance (z_d), discharge ratio (Q_r) (Figure 1), and upstream planform curvature (Ashmore and Parker, 1983; Best, 1987; Biron et al., 1996; Rhoads and Sukholodov, 2004; Boyer et al., 2006; Constantinescu et al., 2012; Ribeiro et al., 2012). Sediment transport through equilibrium confluences, however, is poorly understood (Best and Rhoads, 2008), limiting understanding of how confluences influence local and network-scale patterns of sediment routing.

In this study we assess how coarse bedload particles are routed through equilibrium confluences in a mountain river headwaters. We address two questions: i) How do sediment routing patterns through headwater confluences compare to those described in other, primarily lower-gradient gravel-bed river systems? ii) How do confluences affect the dispersive behavior of coarse bedload particles compared to non-confluence reaches? We address these questions with a tracer experiment conducted through two headwater confluences and a non-confluence control reach. We compare stochastic models of sediment transport and dispersion (Einstein, 1937; Hubbell and Sayre, 1964; Yang and Sayre, 1971) and a dimensionless impulse framework (Phillips et al., 2013) to observed tracer behavior to explore the effects of confluences on sediment routing. We also evaluate our results and their implications in the context of theory regarding confluences and sediment routing through headwater networks. Our study contributes to the growing body of work on particle dispersion and transport dynamics in mountain rivers and is, to our knowledge, the first to investigate these topics with respect to sediment routing through confluences in a field setting.

2 Methods

Here we describe our study area and the preparation, deployment, and measurement of coarse-bedload tracer particles. We then describe the analyses we conducted that allow comparison of

particle displacement through the study confluences to that of the control reach and prior transport studies in gravel-bed river systems. This involved assessment of displacement distributions and a dimensionless impulse, with the goal of evaluating and comparing dispersive regimes. Additional details on these analyses, beyond what is provided below, are in Supplemental Information and Imhoff (2015).

2.1 Study area

We selected a study area in the East Fork Bitterroot (EFB) River basin in western Montana, USA (Figure 2) that is typical of semiarid, snowmelt-dominated, montane headwater systems. This location lacks recent physical disturbances (e.g., post-wildfire debris flows) and contains confluences exhibiting characteristics of the equilibrium morphology described above. The field site drains 298 km^2 of forested and alpine mountainous terrain, in both the Sapphire Mountains and Pintler Range, ranging in elevation from 1584 m to 2895 m. Sediment supplied to channels is comprised of quartzite, argillite, siltite, and feldspathic granitic rock, eroded from metasedimentary Belt Supergroup and Idaho Batholith sources. Annual precipitation is about 0.6 m yr^{-1}, based on data from the Tepee Point weather station 1.4 km from the EFB (Western Regional Climate Center Remote Automated Weather Station, 2015). Runoff is dominated by spring snowmelt, with flows capable of mobilizing coarse bedload typically occurring in similar streams between March and July. Human influences from roads and other land uses are minimal in the study area.

Two tributary confluences mark the upstream and downstream extent of the study area. These are herein referred to as the upper confluence, where Moose Creek and Martin Creek combine, and, 1 km downstream, the lower confluence, where Martin Creek enters the EFB. The tributary and mainstem stream of each study confluence are considered as separate reaches, for the purpose of separately considering incipient motion and transport behavior of tracers starting in each. Between the study confluences is a plane-bed control reach. Combined discharge in the upper confluence is approximately half that of the lower confluence.

Because the site is ungauged, we installed HOBO-U20 water level loggers to record stage at 15-minute intervals during the 2014 study period. One transducer was placed along a surveyed-cross section of the bed at each study reach. We also periodically manually measured water surface elevations and, during wadeable conditions, stream velocities. Above-average flows during the study period reflected that year's large snowpack. Snow water equivalent at SNOTEL sites within 50 km of the study area registered above 150% of normal on 1 April 2014 (http://www.wcc.nrcs.usda.gov/snow/). We estimated the spring 2014 peak flow to have a 3.5 to 4-year recurrence interval, based on transducer data, flood-frequency regression equations developed for western Montana streams (Parrett and Johnson, 2004), and analysis of a downstream US Geological Survey gage. Flood flows peaked between 25 May and 4 June 2014 (Figure 3).

To characterize study-reach morphology, we completed topographic surveys and grain-size measurements. Topography was surveyed using a Leica TS06 total station during the initial tracer deployment (March 2014), before spring runoff high flows, and the summer (July-September) recovery campaign. Topographic surveys entailed longitudinal profiles, to determine slope, and cross-sections at the location of pressure transducers, for use in the incipient motion estimates described below. We also surveyed bedform extents to produce a bedform map. Surface grain size distributions were measured using Wolman pebble counts across each study reach. Channel slopes, dimensions, grain sizes, and confluence characteristics are shown in Table 1 (also see Supplemental Information).

2.2 Bedload tracer preparation, deployment, and measurement

Our study employed passive-integrated transponder (PIT) and radio-frequency identification (RFID) technology for tagging and tracing bedload particles. PIT tags are highly recoverable, durable, and cost-effective relative to other particle tracing methods (e.g., Lamarre et al., 2005; Bradley and Tucker, 2012; Chapuis et al., 2015). Moreover, PIT-tagging allows for analyses of transport of both bed-material populations and specific subsets of the grain population (e.g., by size, shape, lithology), displacement distributions and their evolution over time, and other aspects of transport dynamics.

We collected gravel and cobble particles from Moose Creek, upstream of our study reaches, in January 2014 for tagging. Using a 1-hp drill press, holes 8 mm wide by 30 mm long were drilled using a ~0.8 mm diamond-tipped drill bit. We tagged cobbles with median axes mostly between 60 and 130 mm (Figure 4, Table 2). Many of the tracer particles were larger than the bed D_{50} (Table 1), because particles with b-axes below 45 mm often fractured during drilling. We assumed our tracer particles, which fell within the D_{37} to D_{70} size fraction of bed materials, to be representative of the coarser fraction of mobile bedload particles. The results and interpretation of our sediment tracers thus do not apply for the entire mobile bedload population in this system.

The PIT tags used in this study are 12 mm and 23 mm half-duplex, reour seedad-only tags from Oregon RFID. Vertical read range varies based on tag orientation, battery level, noise proximity, and other factors, but is generally 0.25 to 0.5 m. Previous work has identified horizontal and vertical detection ranges at 0.5 m (Lamarre et al., 2005) and 0.25 m (Bradley and Tucker, 2012). Chapuis et al. (2014) assessed RFID detection ranges and observed higher uncertainty in radial detection distance than reported in other studies. Uncertainty in tracer position is highest for solitary, buried tracers, which are not visible via snorkel survey and have the largest detection radius; clusters of buried tracers, in contrast, have reduced detection ranges via tag interference. We oriented the antenna parallel to the surface of the bed, at a height of about 0.2 m (after Chapuis et al., 2014). For our analysis, we considered tracer movement below the threshold of detection as immobile and assigned a travel distance of 0 m (after Phillips and Jerolmack, 2014). Particles moving beyond the threshold of detection were labeled the "mobile" fraction. In total, 428 cobble and gravel tracers were prepared for deposition into the three study reaches (Table 2).

We installed the PIT-tagged tracers before the onset of the spring snowmelt, in late March and early April 2014. Our seeding method involved loosely seeding tracer particles on the bed surface near the channel thalweg in a grid (Figure 5). Mimicking the arrangement of fluvially-deposited gravels and minimizing the influence of the initial condition of particle deployment is a challenge in tracer studies, but a regular grid such as ours provides a reproducible initial condition and is consistent with previous work (Ferguson and Wathen, 1998). A sparse grid like the one employed here minimizes disturbance to the bed and flow field (Bradley and Tucker,

2012) while simultaneously avoiding "confusing" the PIT tag detection equipment, which encounters issues when dealing with clusters of particles (Chapuis et al., 2014). The gridded surface ranged from 7–13 m wide. We deployed PIT-tagged tracers at equal distances upstream from the confluence in each tributary. Initial tracer positions were recorded using the total station.

Field recovery campaigns to detect tracer locations and measure particle displacement took place after recession of high flows, once the streams were wadeable. The bed was scanned with a 0.5 m diameter loop antenna in conjunction with a backpack reader. Once a tracer was located, the loop antenna was brought towards its detection field from all directions. This helped to identify other tracers in a cluster by reading different tags first, depending on the direction the cluster is approached. Each tracer's position was recorded using the total station. The uncertainty associated with individual total station measurements of tracer position and travel distance is ±0.20 m (Bradley and Tucker, 2012). We also employed a snorkel survey to identify if tracers were buried or clustered together. Visible tracers were occasionally surrounded by other tracers in shallow pockets. At all sites, we scanned with the loop antenna for 200 m downstream of the last detected particle to limit omission of any far-traveling tracers, which influence the tail character of displacement distributions. The position of far-traveling tracers was recorded with a Trimble GEOXH 6000 GPS.

2.3 Particle displacement distributions

To evaluate observed particle displacement distributions across our study site, we tested the applicability of two stochastic models of sediment transport and dispersion: the Einstein-Hubbell-Sayre (EHS; Hubbell and Sayre, 1964) and Gamma-Exponential models (GEM; Yang and Sayre, 1971). These models were chosen following previous tracer experiments, particularly Bradley and Tucker (2012), who tested the fit of the EHS and GEM functions to displacement distributions measured using PIT tags in Halfmoon Creek, Colorado, USA. Halfmoon Creek has similarities in terms of slope, grain size, width, plane-bed morphology, and snowmelt hydrology to our study sites and is thus suitable for comparison with our results. The EHS and GEM models differ by modeling step lengths using either exponential (EHS) or gamma (GEM) distributions, resulting in step-length distributions that decrease monotonically (EHS) or vary more flexibly

(GEM), as described in more detail in Bradley and Tucker (2012) and in our Supplemental Information. We compared EHS and GEM fits to our confluence and non-confluence transport data, with the goal of comparing bulk routing characteristics between the two reach types. In doing so we apply models that approximate step length to test against observed displacement, which for an individual particle may include multiple steps across the 2014 hydrograph.

To further investigate displacement distributions, we assessed dimensionless transport distances of each tracer by scaling each tracer's transport distance (X_i) by its median diameter (D_i). We then calculated normalized transport distance, X_n (after Phillips et al., 2013):

$$X_n = \frac{\frac{X_i}{D_i}}{<\frac{X}{D}>} \quad (1)$$

where (<X/D>) is the mean displacement length for the 2014 flood at each study reach. In addition, we analyzed cumulative exceedance distributions of tracer travel distance for each study reach to assess tail character (after Hassan et al., 2013). This was achieved by measuring the rate of decay of the exceedance distribution tail, P(X>x), where X is a travel distance beyond the user-determined start of the tail, x. The log-log slope of decay (α) distinguishes between heavy-tailed (α < 2) and thin-tailed (α>2) distributions (Metzler and Klafter, 2000; Olinde and Johnson, 2015). We considered <X/D> to be a suitable parameter to test in the context of comparing our tracer data to thin-tailed transport models. These analyses offer a comprehensive approach to investigating whether the overall distribution of particles evolves in a significantly different way when being routed through confluences, as opposed to the plane-bed control reach.

2.4 Dimensionless impulse

We also analyzed tracer data with respect to a cumulative dimensionless impulse I*, that links particle displacement to the duration of flow above the threshold of motion (Phillips et al., 2013), as follows:

$$I^* = \int_{t_i}^{t_f} \frac{(U_e^*)dt}{D_{50}} \quad (2)$$

where t_i and t_f are start and end times, respectively, for flow above a critical threshold of motion of bed materials, and U^*_e is excess shear velocity, which is the difference between the shear velocity (U^*) and the critical shear velocity (U_c^*) associated with initial motion of bed particles. Flume studies have identified that a mobilized sediment particle shows a total displacement that is proportional to U^*_e (Lajeunesse et al., 2010; Martin et al., 2012). Shear velocity is equal to $(gRS)^{0.5}$, where g is gravitational acceleration, R is hydraulic radius, and S is channel slope. For the critical condition (U_c^*), R_c is critical hydraulic radius associated with the mobilization of the average-sized tracer particle and can be back-calculated from critical Shields number (τ_c^*), a non-dimensional shear stress associated with incipient motion of particles in a flow:

$$\tau_c^* = \frac{\rho g R_c S}{(\rho_s - \rho_w) g D_{50}} \quad (3)$$

where ρ_s is sediment bulk density (assumed to equal 2650 kg m^{-3}) and ρ_w is water density (1000 kg m^{-3}).

We used I* to compare tracer transport distances against the cumulative excess shear velocity imparted on grains. We determined I* for each of our five seed reaches and, as a means of comparing confluence and non-confluence reaches, evaluated the extent to which each data set deviated from a linear relationship between <X/D> and I*, which can be considered indicative of a difference in dispersive regimes (Phillips et al., 2013).

Because our tracer equipment could not directly detect initial motion conditions, we estimated τ_c^* using two different empirical approaches, which we selected based on their derivation in gravel-bed systems similar to our study sites and our ability to measure required inputs. For the first estimate, we used Mueller et al.'s (2005) reference dimensionless shear stress relation for steep gravel and cobble-bed rivers:

$$\tau^*_{c,\mathrm{Mueller}} \approx \tau_r^* = 2.18S + 0.021 \quad (4)$$

where τ_r^* is a reference shear stress, which we assume is similar to τ_c^* (after Mueller et al., 2005). One of the study rivers in Mueller et al. (2005), Halfmoon Creek, is similar to our study

site, as described above. For a second estimate of τ_c^*, we used Recking's (2013) mobility shear stress (τ_m^*) equation, which was empirically developed using bedload transport data from gravel-bed transport studies in mountain streams:

$$\tau_{c,Recking}^* \approx \tau_m^* = (5S + 0.06)\left(\frac{D_{84}}{D_{50}}\right)^{4.4\sqrt{S}-1.5}. \quad (5)$$

Analogously to Eq. (5), we assume τ_m^* approximates τ_c^* (after Recking, 2013).

These two estimates for τ_c^* were paired with stage data to estimate the cumulative duration of flow above the threshold of motion, which is difficult to measure directly (Charru et al., 2004). At each seed reach, we used pressure transducer data to identify the critical flow depth (h_c) that corresponds with the R_c for initiating sediment motion, thus linking stage data to estimates of channel-averaged U^* during the 2014 flood hydrograph. Estimates of U^*_e were then integrated across the 2014 hydrograph to estimate I*. Because Eq. (2) is restricted to flow above the threshold of sediment motion, I* limits the frequency-magnitude distribution of U* to conditions relevant to estimated sediment transport and only considers the momentum excess imparted by the flow on sediment particles. This approach adopts the simplifying assumption of a constant U^*_c for a given field site (after Phillips et al., 2013), although we recognize that U^*_c likely varies in both space and time.

3 Results

3.1 Field observations of tracer displacement

We recovered 68–86% of the seeded tracers, depending on the reach (Table 2). Recovery was greatest within study reaches with low D_{84} values and short transport distances, including the control reach and Moose Creek (Table 2). Our recovery rate is comparable to recent tracer studies using RFID technology: 25–78% (Liébault et al., 2012), 93–98% (Bradley and Tucker, 2012), 62–100% (Phillips et al., 2013), 40% (Chapuis et al., 2015).

Similar percentages of recovered tracers (41, 39, and 50%) left each seed reach. At the upper confluence, tracer configurations within the seed reach retained the signature of their gridded spatial pattern in Moose Creek after movement but not in Martin Creek, which contained more boulders to facilitate trapping and clustering of particle tracers (Figure 5). Particles seeded in Moose Creek also constituted the majority of tracers exported into the confluence itself. Deposition within the confluence primarily correlated to depositional bars flanking the scour hole (Figure 6). Particles deposited within the scour hole were segregated by contributing stream. Tracers from the upper confluence seed reaches had short travel distances and, even after being mobilized, remained within the confluence zone (Figure 6).

Particles recovered in the lower confluence largely retained the signature of the gridded arrangement of their initial positioning at both seed reaches, even after mobilization. The relative contribution of tracers into the confluence was more evenly distributed than in the upper confluence: 55% of deposited tracers came from the East Fork, with the remaining 45% from Martin Creek. Similar to the upper confluence, tracer particles remained segregated as they progressed through the confluence, stranding preferentially on bank-attached depositional bars. Deposition within the scour hole was limited and segregated, further agreeing with the upper confluence. An additional group of tracers, seeded at the upstream junction corner, were immobile. Similar to the upper confluence, large boulders were effective in trapping mobile tracer particles. Of the recovered tracers in the entire lower confluence, 23% left the confluence zone completely, with 58% of post-confluence tracers originating in the East Fork and 42% from Martin Creek. Recovered particles downstream of the lower confluence cease to be segregated after about 30 m, and were recovered approximately in the channel center.

3.2 Particle displacement distributions

The Einstein-Hubbell Sayre (EHS) and Yang-Sayre (GEM) models provided similar-quality fits to each other in all study reaches (Figure 7). The Yang-Sayre GEM provides the most accurate fit, with a slight R^2 advantage ranging from 0.01 to 0.001. Both the EHS and GEM models accurately approximate the slowest-moving tracer bins, generally overestimate the probabilities of mid-range bins, and underestimate the probabilities of fast-moving bins that correspond to the

tail of the displacement probability distribution. In the control reach, fast tracer bins generally have a smaller residual than in the confluence study reaches. The models fit the lower confluence tracers better than the upper confluence tracers (Table 3). In all reaches but Martin Creek (lower confluence), the average transport distance of our data exceeded model estimates (Table 3).

At the upper confluence, mobile tracers entering the confluence zone exhibited a distinct step in the spatial distribution of tracer positions, denoting enhanced transport and reduced depositional probabilities (Figure 8, after Haschenburger, 2013). Enhanced transport is also evident for tracers routing through the lower confluence reaches (Figure 8): a distinct step is evident for tracers entering the confluence, where the probability of deposition decreases for the duration of time spent within the confluence zone. The control reach lacks significant steps and instead features a smooth decay indicative of consistent depositional rates with distance downstream.

Dimensionless displacement distributions deviate from a best-fit exponential distribution at distances beyond approximately twice the average normalized transport distance (Figure 9). In evaluating X_n, tracers in the upper confluence reaches do not travel as far relative to the population mean as those in other seed reaches. Tail character in confluence populations generally showed smaller α values than the control reach, corresponding to heavier tails and greater dispersive growth (Figure 10). The point of origin of the tail is user-defined, however, and varying the start point changes the resulting slope of the exceedance tail. We therefore assessed tail character at multiple points above the 75^{th} percentile of tracer displacement distance, to test the sensitivity of tail designation. None of the study reaches cross the thin-heavy threshold (α=2) by varying the tail start point. We thus chose to define the tail as beginning at the 80^{th} tracer percentile. Only Moose Creek shows a thinner tail in the exceedance probability distribution than the control reach. Martin Creek (at both the upper and lower confluences) exhibits a heavy-tail, while Moose Creek, the control reach, and East Fork Bitterroot are thin-tailed. The data do not distinguish whether transport through confluences is thin or heavy-tailed, rather suggesting that distributions of tracers moving through confluences are generally "heavier" and exhibit a higher proportion of tracers traveling far distances than in the plane-bed reach.

3.3 Dimensionless impulse

Our estimates of critical Shields number ranged from 0.056 to 0.109 (Table 4), slightly larger than often-assumed values of τ_c^* (e.g., τ_c^*=0.045; Church, 2006). For all study reaches, $\tau^*_{c,Mueller}$ values (Eq. 4) were lower than the $\tau^*_{c,Recking}$ values (Eq. 5), resulting in correspondingly lower U^*_c values. These calculations indicate that flow exceeded the threshold of motion for 8–37 ($\tau^*_{c,Mueller}$) or 1–17 ($\tau^*_{c,Recking}$) days, with the lower confluence experiencing the longest duration above the critical level. The distribution of U* and I* scale with channel dimensions and peak discharge, with the upstream confluence seed reaches experiencing smaller U* and I* values than the control reach and lower confluence (Table 4). Moose Creek, for example, is wider and shallower than Martin Creek at the upper confluence, and requires a larger discharge increase to move from the Mueller to Recking incipient motion threshold estimate. This results in reach-specific variation in sensitivity to the estimation method for incipient motion. We found that I* scaled well with tracer displacement (Table 4) and confirmed its usefulness for assessing coarse particle transport at the EFB.

We found <X/D> to conform to a linear relation to I*, and variance (σ^2) to a power-law function, in agreement to the predictions and findings of Phillips et al. (2013) and Phillips and Jerolmack (2014) regarding the broad applicability of normalized travel distances and impulse for characterizing bedload transport (Figure 11). The occurrence of a linear fit supports the notion that I* may be used to correlate flow strength with travel distance across multiple sites. However, a linear fit through the origin was far less appropriate than that found by Phillips et al. (2013). Fits could be greatly improved when only considering the relationship between confluence reaches: the control reach has similar displacement but higher I* values than reaches at the upper confluence, giving it the highest residual from the best-fit curve in both cases. We did not normalize I* by frictional resistance, as it did not prove to significantly improve the collapse of our tracer data.

4 Discussion

4.1 Coarse sediment routing through confluences

Our study used PIT / RFID technology to provide novel insights into the effect of tributary confluences on sediment routing through mountain streams. Maximum transport distances along scour-hole flanks and segregation are similar to the findings of Mosley (1976) and Best (1988). Because we detect no tracers beyond the extent of the upper confluence, we take the depositional pattern in Figure 6 to reflect a tendency of our tracers to route along, rather than through, the scour hole. We see similar depositional patterns for tracers that were detected within the lower confluence and posit that similar transport corridors apply. We consider these transport patterns to reflect the controlling influences of Θ and Q_r; the simple upstream planform geometry and minimal bed discordance (z_d) at our sites suggest that those factors exert little influence on morphodynamics in our study confluences. Observed discordance between scour and tributary mouth bars at our study confluences (0.6 and 1.4 m, respectively) exceed that of Roy and Bergeron (1990; ~0 m at Θ=15), supporting observations that scour is largely absent at low Θ values (Benda and Cundy, 1990).

Our data also agree with the assertions of Best (1988) and others as to how the position and orientation of the scour hole is influenced by Q_r. Increased penetration of flow from the tributary at the upper confluence, due to higher Q_r, forced the scour hole towards the middle of the confluence, as opposed to the lower confluence where the scour was shifted by greater discharge from the East Fork Bitterroot. Observed feedbacks between confluence morphology and particle transport suggest similar confluence morphodynamics as observed in past studies (e.g., Mosley, 1976; Best, 1987; Boyer et al., 2006; Rhoads et al., 2009), though in a higher-gradient, more headwaters setting than previous work.

4.2 Effects of confluences on dispersion

Fit quality of the EHS and GEM models support Bradley and Tucker's (2012) assertion that a gamma or exponential distribution can approximate the compound Poisson distribution of coarse tracer displacement in headwater systems. Differences between the EHS and GEM at our site are almost indistinguishable, whereas Bradley and Tucker (2012) found that the GEM described observed step lengths than the monotonically decreasing EHS. The strong fits of the EHS and GEM may reflect the short duration (one flood) of our study; Bradley and Tucker (2012)'s study

spanned four flood events. The quality of these fits is likely to weaken over time as particles become vertically integrated with the bed (Haschenburger, 2013).

General accordance to the EHS and GEM models suggests that a thin-tailed model may be reasonable for describing particle displacement distributions through confluences as well as in our control reach. The linear collapse in semi-log space observed in Figure 9 further supports this view, indicating that normalized transport distance (Eq. 1) may serve as an appropriate single-parameter approach to describe tracer displacement at the scale of individual floods. However, the tail of the distribution diverges from the model fits and exponential regression. This divergence is evident in our other analyses, which suggest relatively heavy-tailed displacement distributions and reduced depositional probabilities for coarse sediment within the confluence zone. Enhanced transport is further suggested by larger transport distances for a given impulse (Table 4; Figure 10). We therefore assert that coarse particles entering the confluence zone are less likely to deposit than in the preceding plane bed reach, and that particles exposed to the greater dimensionless impulse beyond the confluence travel farther distances than those that do not enter the confluence.

4.3 Confluences and large-scale sediment routing

We therefore propose a conceptual model where equilibrium confluences have the effect of enhancing coarse bedload transport and dispersion downstream. Tracers moving through confluences show greater transport distances for a given I* and reduced depositional probabilities in the confluence itself. This would distort the spatial distribution of a population of coarse particles in the Lagrangian field perspective, where front-runner tracers are preferentially routed through confluences and the overall spatial distribution distorted in the downstream direction. Tracer transport dynamics were reasonably well-fitted by thin-tailed models, but not for far-traveling tracers. The differences we observe between confluence and non-confluence reaches are subtle, but this effect may increase as particles are routed through successive confluences.

490 This conceptual model applies to confluence morphology that is governed by hydraulics and
491 sediment supply typical of snowmelt-dominated hydrographs, as opposed to confluences
492 influenced by recent disturbance. We consider our model within the context of Benda et al.'s
493 (2004) Network Variance Model, to consider the effects of confluences at the scale of headwater
494 river networks. The NVM considers that the likelihood of morphologically significant
495 perturbations to mainstem channels, in the form of large sediment deposits, increases in the
496 vicinity of confluences due to upstream disturbance. Our sites, where recent tributary
497 disturbances are absent, diverge from this model, such that sediment can propagate, unhindered
498 by recent sediment deposits, through confluence zones, and indeed, transport is enhanced rather
499 than impeded across our equilibrium confluences. Our work expands, rather than refutes, the
500 NVM by suggesting that confluences play morphologically important roles with respect to
501 sediment routing both in and outside of disturbance-dominated headwater systems.
502
503 We hypothesize, based on our findings above, that sediment routing through individual
504 equilibrium confluences influences routing at the larger basin scale in mountain watersheds. As
505 the equilibrium confluence is contingent on high Q_r, Θ, and other physical controls, we would
506 expect certain basin types to accumulate confluence effects to a greater extent than others,
507 according to basin shape, drainage density, and network geometry (Benda et al., 2004). As an
508 illustrative example, we compare the EFB basin to a similarly sized basin (Tin Cup Creek), 35
509 km to the west in the Bitterroot Range (Figure 12). The morphology of basins in the Bitterroot
510 versus Sapphire Mountains differs considerably as a result of differences in erosive history and
511 lithology. The Bitterroot are formerly glaciated and have granitic rock, with U-shaped valleys,
512 elongate basins, and trellis drainage networks. The unglaciated Sapphires, in contrast, have V-
513 shaped valleys, compact basins, and dendritic networks. Comparing these basin types, basins
514 such as those in the Sapphire Range (e.g., the upper EFB basin) have larger tributary channels of
515 increasing order (Strahler, 1952), where tributary discharges scale with increased mainstem flow,
516 and a greater number and downstream extent of equilibrium confluences than the elongate basins
517 (Benda et al., 2004) that largely define basins such as the Bitterroot. This suggests that basin
518 shape, itself a function of lithology and climate, may inform the dispersive behavior of a coarse
519 bedload population in locations lacking recent disturbance and corresponding confluence

deposits. This would determine the setting where confluences would be expected to enact a cumulative and significant effect on coarse sediment transport.

Understanding the extent to which equilibrium confluences affect basin-scale routing requires further insight into coarse bedload connectivity in mountain rivers. Our conceptual model assumes steady progression of coarse sediment downstream in a plane-bed morphology; however, discontinuity in coarse sediment transfer can emerge when competence is reduced and particles enter long-term storage (e.g., Tooth et al., 2002; Hooke, 2003; Fryirs, 2013; Bracken et al., 2015). Certain channel morphologies exhibit bedload particle displacements between morphologic units (e.g., bars; Pyrce and Ashmore, 2003), which can result in disconnectivity if bedform-scale aggradation exceeds rates of removal (Hooke, 2003). The unique dispersive patterns we observe at the scale of individual confluences must be analyzed across multiple confluences, over multiple floods, and within other channel morphologies, to quantify the extent of their influence over large-scale patterns of sediment routing.

5 Conclusion

Our tracer study, the first to date of coarse-sediment routing through mountain-river confluences, showed that in gravel-bed headwater systems, tributary confluences represent geomorphically unique locations that locally affect patterns of sediment routing. At the reach scale, coarse sediment is routed through confluences along the flanks of a well-defined scour hole, in agreement with observations and flume studies from other gravel-bed systems. Transport distance of mobilized clasts through the confluence zone is less dependent on grain size than in the plane-bed channel morphology, especially for larger grains. Distributions of particle displacement were along the thin-heavy tail threshold; longer-term monitoring would elucidate the evolution of tail characteristics. Regardless of thin or heavy-tailed transport, confluence reaches generally featured a “heavier” distribution of displacement distances and a greater proportion of tracers in the tail. We therefore found confluence reaches to impart greater transport distances and dispersive growth compared to the plane-bed channel morphology, even when particles did not progress beyond the downstream extent of the confluence itself. Our study

also illustrates the utility of tracer studies using PIT / RFID technology for providing field-based insights into sediment transport dynamics.

We proposed a conceptual model where equilibrium headwater confluences alter patterns of dispersion and enhance downstream transport. According to the sediment cascade framework of Fryirs (2013), this would classify equilibrium confluences as an enhanced longitudinal linkage compared to the plane-bed channel morphology. Combined with the work of Benda et al. (2004) and others, we suggest that the location of confluences influences sediment routing patterns and, in the case of upstream disturbances, responses to sediment pulses, in headwater systems both with and without disturbance-derived sediment deposits. Longer-term sediment transport studies across confluence and non-confluence reaches, combined with analysis of changes in bed elevation and texture in intervening reaches to place the work in a mass conservation framework, would further clarify sediment routing patterns in mountain channel networks and thus inform a range of problems, including solid-phase contaminant transport (Bradley et al., 2010), cosmogenic radionuclide accumulation (Gayer et al., 2008), sediment budgeting (Malmon et al., 2005), and the duration and topographic impact of pulses on aquatic habitat (Lisle et al., 2001).

Acknowledgments

We thank P.A. Duvillard, A. Maphis, D. Davis, M. Jahnke, and A. Sawyer for field assistance; M. Hassan, L. Eby, M. Maneta, S. Bywater-Reyes, and R. Manners for insight in the planning and implementation of this work; N. Bradley and C. Legleiter for aid in model use and coordinate transformation; and C. Phillips for assistance in performing impulse analyses. Comments from two anonymous reviewers greatly improved the manuscript. This work was supported by the Montana Institute on Ecosystems' award from the National Science Foundation EPSCoR Track-1 program under Grant # EPS-1101342, and by the Montana Geological Society, the Geological Society of America, and the Northwest Scientific Association.

References

Ashmore, P. and Parker, G.: Confluence scour in coarse braided streams, Water Resour. Res., 19, 392–402, 1983.

Benda, L. and Cundy, W.: Predicting deposition of debris flows in mountain channels, Can. Geotech. J., 27, 409–417, 1990.

Benda, L. and Dunne, T.: Stochastic forcing of sediment routing and storage in channel networks, Water Resour. Res., 33, 2865–2880, 1997.

Benda, L., Andras, K., Miller, D., and Bigelow, P.: Confluence effects in rivers: Interactions of basin scale, network geometry, and disturbance regimes, Water Resour. Res., 40, W05402, doi:10.1029/2003WR002583, 2004.

Best, J.: Flow dynamics at river channel confluences: implications for sediment transport and bed morphology, Soc. Econ. Paleontol. Minearologists, 39, 27–35, 1987.

Best, J.: Sediment transport and bed morphology at river channel confluences, Sedimentology, 35, 481–498, 1988.

Best, J.L., and Rhoads, B.L.: Sediment transport, bed morphology and the sedimentology of river channel confluences, in: River Confluences, Tributaries and the Fluvial Network, JohnWiley and Sons, Chichester, UK, 2008.

Biron, P., Best, J.L., Roy, A.G.: Effects of bed discordance on flow dynamics at open channel confluences, J. Hydraul. Eng., 122, 676–682, 1996.

Boyer, C., Roy, A.G., and Best, J.: Dynamics of a river channel confluence with discordant beds: Flow turbulence, bed load sediment transport, and bed morphology, J. Geophys. Res., 111, F04007, doi:10.1029/2005JF000458, 2006.

603 Bracken, L. J., Turnbull, L., Wainwright, J. and Bogaart, P.: Sediment connectivity: a framework
604 for understanding sediment transfer at multiple scales, Earth Surf. Process. Landforms, 40,
605 177–188, doi:10.1002/esp.3635, 2015.

606 Bradley, N. and Tucker, G.E.: Measuring gravel transport and dispersion in a mountain river
607 using passive radio tracers, Earth Surf. Process. Landf., 37,1034–1045,
608 doi:10.1002/esp.3223, 2012.

609 Bradley, D.N., Tucker, G.E., and Benson, D. A.: Fractional dispersion in a sand bed river. J.
610 Geophys. Res., 115, F00A09, doi:10.1029/2009JF001268, 2010.

611 Brooks, A. and Brierley, G.: Geomorphic responses of lower Bega River to catchment
612 disturbance, 1851-1926, Geomorphology, 18, 291-304, 1997.

613 Chapuis, M., Bright, C.J., Hufnagel, J., and MacVicar, B.: Detection ranges and uncertainty of
614 passive Radio Frequency Identification (RFID) transponders for sediment tracking in gravel
615 rivers and coastal environments, Earth Surf. Process. Landf., 39, 2109–2120,
616 doi:10.1002/esp.3620, 2014.

617 Chapuis, M., Dufour, S., Provansal, M., Couvert, B., and de Linares, M.: 2015. Coupling channel
618 evolution monitoring and RFID tracking in a large, wandering, gravel-bed river: Insights
619 into sediment routing on geomorphic continuity through a riffle–pool sequence,
620 Geomorphology, 231, 258–269, doi:10.1016/j.geomorph.2014.12.013, 2015.

621 Charru, F., Mouilleron, H., and Eiff, O.: Erosion and deposition of particles on a bed sheared by
622 a viscous flow, J. Fluid Mech., 519, 55–80, doi:10.1017/S0022112004001028, 2004.

623 Church, M.: Geomorphic thresholds in riverine landscapes, Freshw. Biol., 47, 541–557,
624 doi:10.1046/j.1365-2427.2002.00919.x, 2002.

625 Church, M.: Bed material transport and the morphology of alluvial river channels, Annu. Rev.
626 Earth Planet. Sci., 34, 325–354, doi:10.1146/annurev.earth-33.092203.122721, 2006.

627 Constantinescu, G., Miyawaki, S., Rhoads, B. L., and Sukhodolov, A.: Numerical analysis of the
628 effect of momentum ratio on the dynamics and sediment-entrainment capacity of coherent
629 flow structures at a stream confluence, J. Geophys. Res., 117, F04028,
630 doi:10.1029/2012JF002452, 2012.

631 Einstein, H.A.: Bed load transport as a probability problem, Ph.D., ETH Zurich, 1937.

632 Ferguson, R. and Wathen, S.: Tracer-pebble movement along a concave river profile : Virtual
633 velocity in relation to grain size and shear stress transport and deposition, Water Resour.
634 Res., 34, 2031–2038, 1998.

635 Ferguson, R., Cudden, J.R., Hoey, T.B., and Rice, S.P.: River system discontinuities due to
636 lateral inputs: generic styles and controls, Earth Surf. Process. Landforms, 31, 1149–1166,
637 doi:10.1002/esp.1309, 2006.

638 Fryirs, K.: (Dis)Connectivity in catchment sediment cascades: a fresh look at the sediment
639 delivery problem, Earth Surf. Process. Landf., 38, 30–46, doi:10.1002/esp.3242, 2013.

640 Gayer, E., Mukhopadhyay, S., and Meade, B.J.: Spatial variability of erosion rates inferred from
641 the frequency distribution of cosmogenic 3He in olivines from Hawaiian river sediments,
642 Earth Planet. Sci. Lett., 266, 303–315, doi:10.1016/j.epsl.2007.11.019, 2008.

643 Gomi, T., Sidle, R.C., and Richardson, J.S.: Understanding processes and downstream linkages
644 of headwater systems, Bioscience, 52, 905-916,
645 doi:10.1641/00063568(2002)052[0905:UPADLO]2.0.CO;2, 2002.

646 Haschenburger, J.K.: Tracing river gravels: Insights into dispersion from a long-term field
647 experiment, Geomorphology, 200, 121–131, doi:10.1016/j.geomorph.2013.03.033, 2013.

648 Hassan, M.A., Church, M., and Schick, A.P.: Distance of movement of coarse particles in gravel
649 bed streams, Water Resour. Res., 27, 503–511, 1991.

650 Hassan, M. A., Voepel, H., Schumer, R., Parker, G., and Fraccarollo, L.: Displacement
651 characteristics of coarse fluvial bed sediment, J. Geophys. Res. Earth Surf., 118, 155–165,
652 doi:10.1029/2012JF002374, 2013.

653 Hoffman, D.F. and Gabet, E.J.: Effects of sediment pulses on channel morphology in a gravel-
654 bed river, Geol. Soc. Am. Bull., 119, 116–125, doi:10.1130/B-25982.1, 2007.

655 Hubbell, D. and Sayre, W.: Sand transport studies with radioactive tracers, J. Hydraul. Div., 90,
656 39–68, 1964.

657 Imhoff, K.I.: Sediment routing through channel confluences: Particle tracing in a gravel-bed
658 river headwaters, M.S. thesis, University of Montana, Missoula, MT, 2015.

659 Kasprak, A., Wheaton, J.M., Ashmore, P.E., Hensleigh, J.W., and Peirce, S.: The relationship
660 between particle travel distance and channel morphology : Results from physical models of
661 braided rivers, J. Geophys. Res. Earth Surf., 120, 55–74, http://doi:10.1002/2014JF003310,
662 2014.

663 Knighton, A.D.: Longitudinal changes in size and sorting of stream-bed material in four English
664 rivers, Geol. Soc. Am. Bull., 91, 55-62, 1980.

665 Lajeunesse, E., Malverti, L., and Charru, F.: Bed load transport in turbulent flow at the grain
666 scale: Experiments and modeling, J. Geophys. Res., 115, F04001, doi:10.1029/2009-
667 JF001628, 2010.

668 Lamarre, H., MacVicar, B., and Roy, A. G.: Using passive integrated transponder (PIT) tags to
669 investigate sediment transport in gravel-bed rivers, J. Sediment. Res., 75, 736–741,
670 doi:10.2110/jsr.2005.059, 2005.

671 Lancaster, S.T. and Casebeer, N.E.: Sediment storage and evacuation in headwater valleys at the
672 transition between debris-flow and fluvial processes, Geology, 35, 1027-1030,
673 doi:10.1130/G239365A.1, 2007.

674 Liébault, F., Bellot, H., Chapuis, M., Klotz, S., and Deschâtres, M.: Bedload tracing in a high-
675 sediment-load mountain stream, Earth Surf. Process. Landforms, 37, 385–399,
676 doi:10.1002/esp.2245, 2012.

677 Lisle, T.E., Cui, Y., Parker, G., Pizzuto, J.E., and Dodd, A.M.: The dominance of dispersion in
678 the evolution of bed material waves in gravel-bed rivers, Earth Surf. Process. Landforms,
679 26, 1409–1420, doi:10.1002/esp.300, 2001.

680 Malmon, D. V., Reneau, S.L., Dunne, T., Katzman, D., and Drakos, P.G.: Influence of sediment
681 storage on downstream delivery of contaminated sediment, Water Resour. Res., 41, 1–17,
682 doi:10.1029/2004WR003288, 2005.

683 Martin, R. L., Jerolmack, D.J., and Schumer, R.: The physical basis for anomalous diffusion in
684 bed load transport, J. Geophys. Res., 117, F01018, doi:10.1029/2011JF002075, 2012.

685 Metzler, R., and Klafter, J.: The random walk's guide to anomalous diffusion: a fractional
686 dynamics approach, Physics Reports, 339, 1-77, doi:10.1016/S0370-1573(00)000703, 2000.

687 Milan, D. J.: Sediment routing hypothesis for pool-riffle maintenance, Earth Surf. Process.
688 Landforms, 38, 1623–1641, doi:10.1002/esp.3395, 2013.

689 Montgomery, D. R and Buffington, J.M.: Channel-reach morphology in mountain drainage
690 basins, Geol. Soc. Am. Bull., 109, 596–611, 1997.

691 Mosley, M.P.: An experimental study of channel confluences, J. Geol., 84, 535–562, 1976.

692 Mueller, E.R., Pitlick, J., and Nelson, J.M.: Variation in the reference Shields stress for bed load
693 transport in gravel-bed streams and rivers, Water Resour. Res., 41, F02016,
694 doi:10.1029/2004WR003692, 2005.

695 Nikora, V., Habersack, H., Huber, T., and McEwan, I.: On bed particle diffusion in gravel bed
696 flows under weak bed load transport, Water Resour. Res., 38, 9 pp.,
697 doi:200210.1029/2001WR000513, 2002.

698 Olinde, L., and Johnson, J.P.L.: Using RFID and accelerometer-embedded tracers to measure
699 probabilities of bed load transport, step lengths, and rest times in a mountain stream, Water
700 Resour. Res., 51, 7572-7589, doi:10.1002/2014WR016120, 2015.

701 Parrett, C., and Johnson, D.R.: Methods for estimating flood frequency in Montana based on data
702 through water year 1998, USGS Water-Resources Investigations Rep. 03-4308, Reston,
703 VA, 2004.

704 Phillips, C.B. and Jerolmack, D.J.: Dynamics and mechanics of bed-load tracer particles, Earth
705 Surf. Dyn., 2, 513–530, doi:10.5194/esurf-2-513-2014, 2014.

706 Phillips, C.B., Martin, R.L., and Jerolmack, D.J.: Impulse framework for unsteady flows reveals
707 superdiffusive bed load transport, Geophys. Res. Lett., 40, 1328–1333,
708 doi:10.1002/grl.50323, 2013.

709 Prosser, I.P., Rutherfurd, I.D., Olley, J.M., Young, W.J., Wallbrink, P.J., and Moran, C.J.: Large-
710 scale patterns of erosion and sediment transport in river networks, with examples from
711 Australia, Mar. Freshw. Res., 52, 81–99, doi:10.1071/MF00033_CO, 2001.

712 Pyrce, R. S., and Ashmore, P.E.: The relation between particle step length distributions and
713 channel morphology in gravel-bed streams: a synthesis, Geomorphology, 56, 167–187,
714 doi:10.1016/S0169-555X(03)00077-1, 2003.

715 Recking, A.: Simple method for calculating reach-averaged bed-load transport, J. Hydraul. Eng.,
716 139, 70–75, doi:10.1061/(ASCE)HY.1943-7900.0000653, 2013.

717 Rhoads, B.L.: Changes in stream channel characteristics at tributary junctions. Phys. Geogr., 8,
718 346–361, doi:10.1080/02723646.1987.10642333, 1987.

719 Rhoads, B.L. and Sukhodolov, A.N.: Spatial and temporal structure of shear layer turbulence at a
720 stream confluence, Water Resour. Res., 40, doi:10.1029/2003WR002811, 2004.

721 Rhoads, B.L., Riley, J.D., and Mayer, D.R.: Response of bed morphology and bed material
722 texture to hydrological conditions at an asymmetrical stream confluence, Geomorphology,
723 109, 161–173, doi:10.1016/j.geomorph.2009.02.029, 2009.

724 Ribeiro, M.L., Blanckaert, K., Roy, A. G., and Schleiss, A. J.: Flow and sediment dynamics in
725 channel confluences, J. Geophys. Res., 117, F01035, doi:10.1029/2011JF002171, 2012.

726 Rice, S.P., Greenwood, M.T., and Joyce, C.B.: Tributaries, sediment sources, and the
727 longitudinal organisation of macroinvertebrate fauna along river systems, Can. J. Fish.
728 Aquat. Sci., 58, 824–840, doi:10.1139/cjfas-58-4-824, 2001.

729 Richards, K.S.: A note on changes in channel geometry at tributary junctions, Water Resour.
730 Res., 16, 241–244, doi:10.1029/WR016i001p00241, 1980.

731 Roy, A.G. and Bergeron, N.: Flow and particle paths at a natural river confluence with coarse
732 bed material, Geomorphology, 3, 99–112, doi:10.1016/0169555X(90)90039S, 1990.

733 Sklar, L. S., Fadde, J., Venditti, J.G., Nelson, P., Wydzga, M.A., Cui, Y., and Dietrich, W.E.:
734 Translation and dispersion of sediment pulses in flume experiments simulating gravel
735 augmentation below dams, Water Resour. Res., 45, W08439, doi:10.1029/2008WR007346,
736 2009.

737 Strahler, A.N.: Hypsometric (area-altitude) analysis of erosional topography, Geol. Soc. Am.
738 Bull., 63, 1117-1142, doi:10.1130/00167606(1952)63[1117:HAAOET]2.0.CO;2, 1952.

739 Swanson, F.J. and Fredriksen, R.L.: Sediment routing and budgets : Implications for judging
740 impacts of forestry practices, in: Sediment Budgets and Routing in Forested Drainage
741 Basins, Swanson, F.J., Janda, R.J., Dunne, T., Swanston, D.N., U.S. Forest Service,
742 Portland, OR, 129-137, 1982.

743 Swanson, B. J., and Meyer, G.: Tributary confluences and discontinuities in channel form and
744 sediment texture: Rio Chama, NM, Earth Surf. Process. Landforms, 39, 1927–1943,
745 doi:10.1002/esp.3586, 2014.

746 Tooth, S., McCarthy, T.S., Brandt, D., Hancox, P.J., and Morris, R.: Geological controls on the
747 formation of alluvial meanders and floodplain wetlands: the example of the Klip River,
748 eastern Free State, South Africa, Earth Surf. Process. Landforms, 27, 797–815,
749 doi:10.1002/esp.353, 2002.

750 Yang, C. and Sayre, W.: Stochastic model for sand dispersion. J. Hydraul. Div., 97, 265–288,
751 1971.

Tables

Table 1: Channel morphology and bed-material grain-size characteristics at each study reach. Width and depth values are bankfull dimensions, as measured along surveyed cross-sections; Q_r, θ, and z_d are illustrated and defined in Figure 1. Upper and lower confluences reaches are denoted with (U) and (L), respectively.

Study Reach	**S**	**Width (m)**	**Depth (m)**	**D_{50} (m)**	**D_{84} (m)**	**Q_r[a] (avg)**	**Θ**	**z_d (m)**
Moose Creek (U)	0.018	11	0.76	0.05	0.10	0.63	8	0.16
Martin Creek (U)	0.029	7	0.94	0.06	0.15		6°	
Control Reach	0.016	15	0.78	0.06	0.13	–	–	–
Martin Creek (L)	0.017	15	0.80	0.07	0.12	0.45	8	0
East Fk. Bitterroot (L)	0.016	16	1.03	0.07	0.14		1°	

[a] calculated by dividing the smaller trunk stream by volume over the mainstem. Qr = Q(Moose)/Q(Martin) in the upper confluence, and Q(Martin)/Q(East Fork) in the lower confluence.

763 Table 2: Tracer recovery and transport statistics by study reach

Study Reach	n^a	$n_{rec}{}^b$	Recovery (%)	D_{50} (m)	$(X \pm \sigma)_{tot}$ (m)[c]	$(X \pm \sigma)_{mob}$ (m)	X_{max} (m)
Moose Creek (U)	65	53	82	0.077	7.4±6.6	8.5±6.4	24.5
Martin Creek (U)	62	42	68	0.081	3.8±4.1	4.4±4.1	20.6
Control Reach	97	83	86	0.080	4.2±5.3	4.9±5.4	22.7
Martin Creek (L)	103	71	68	0.082	14.6±22.9	16.4±24	133
East Fk. Bitterroot (L)	101	74	73	0.080	47.4±56.3	49.4±56.6	211

764 [a] number of tracers deployed

765 [b] number of tracers recovered

766 [c] X is average transport distance, σ is standard deviation

767 * "tot" and "mob" describe (1) the total tracer population and (2) tracers moving beyond 0.5 meters

768

769 Table 3: Tracer statistics derived from two stochastic models of tracer transport and dispersion:
770 Einstein-Hubbell-Sayre (EHS) and the Yang-Sayre Gamma Exponential Model (GEM).

	EHS			GEM		
Study Reach	**X**	**σ**	**CV**[a]	**X**	**σ**	**CV**
Moose Creek (U)	6.7	5.7	0.86	6.6	5.7	0.87
Martin Creek (U)	3.8	3.8	1.0	3.8	3.9	1.0
Control Reach	4.2	4.6	1.1	4.2	4.6	1.1
Martin Creek (L)	15.6	24.6	1.6	16.2	25.1	1.6
East Fk. Bitterroot (L)	43.9	61.4	1.4	43.7	61.0	1.4

771 [a] coefficient of variation

772 [b] The values presented here incorporate estimates of critical Shields stress calculated from Eq. 4 (Mueller et al.,
773 2005); results are nearly identical if Eq. 6 is used instead.

774

775 Table 4: Critical shear velocity (U_c*) and dimensionless impulse (I*) at each study reach.

	$\tau^*_{c,Mueller}$			$\tau^*_{c,Recking}$		
Study Reach	τ^*_c	U^*_c **(m/s)**	I^*	τ^*_c	U^*_c **(m/s)**	I^*
Moose Creek (U)	0.06	0.23	602000	0.08	0.27	14900
Martin Creek (U)	0.08	0.29	310000	0.11	0.34	37600
Control Reach	0.06	0.23	425000	0.07	0.25	88400
Martin Creek (L)	0.06	0.25	1200000	0.09	0.31	86000
East Fk. Bitterroot (L)	0.06	0.25	1900000	0.07	0.29	577000

776

777

Figures

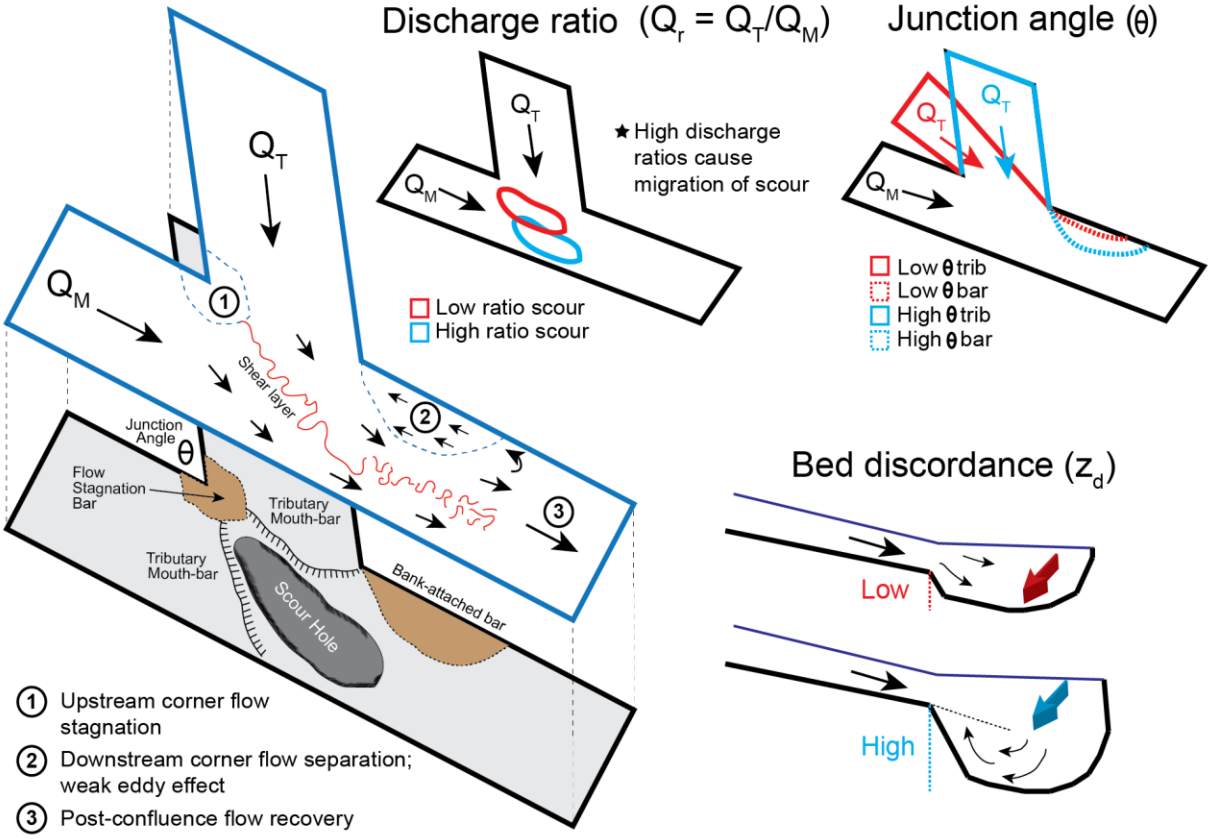

Figure 1: Flow (top left) and morphology (bottom left) in a gravel-bed confluence (after Best, 1987). Key variables influencing hydraulics and morphology include discharge ratio (Q_r), junction angle (θ), bed discordance (z_d), and upstream planform geometry (not pictured).

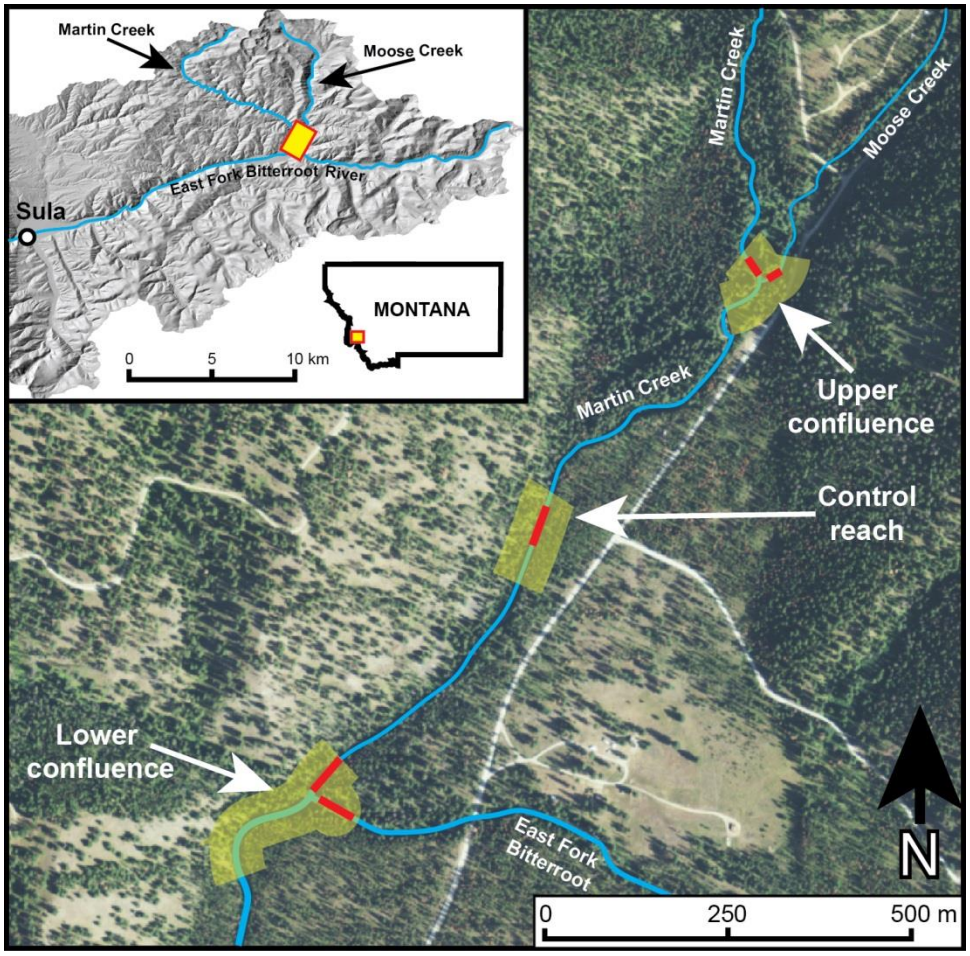

Figure 2: Study area, including location within the East Fork Bitterroot River's headwaters (upper left) and three study sites: upper and lower confluences and a control reach, outlined in yellow; individual reaches in which PIT-tagged particles were seeded are outlined in red.

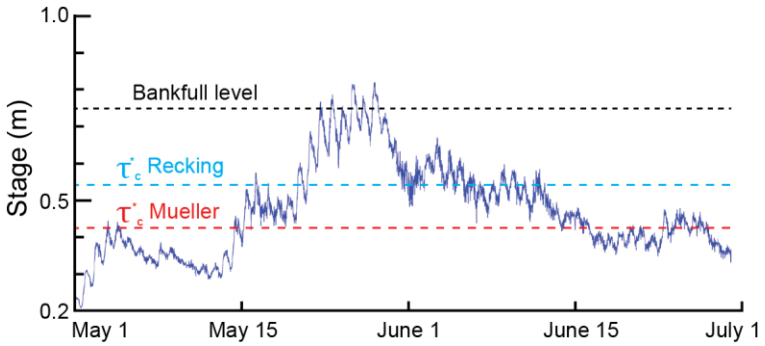

Figure 3: Stage hydrograph during spring 2014 runoff period at lower confluence (East Fork Bitterroot River) study site. Estimated bankfull level, based on cross-section topography surveyed at transducer location, is shown as horizontal dotted line.

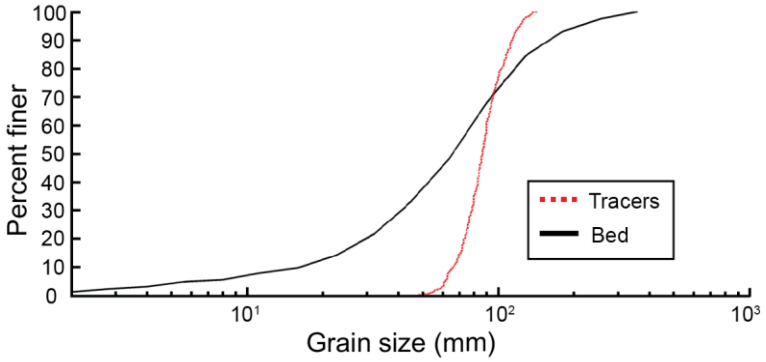

Figure 4: Grain size distribution of tagged tracers (red) and streambed (black) composite over all study sites.

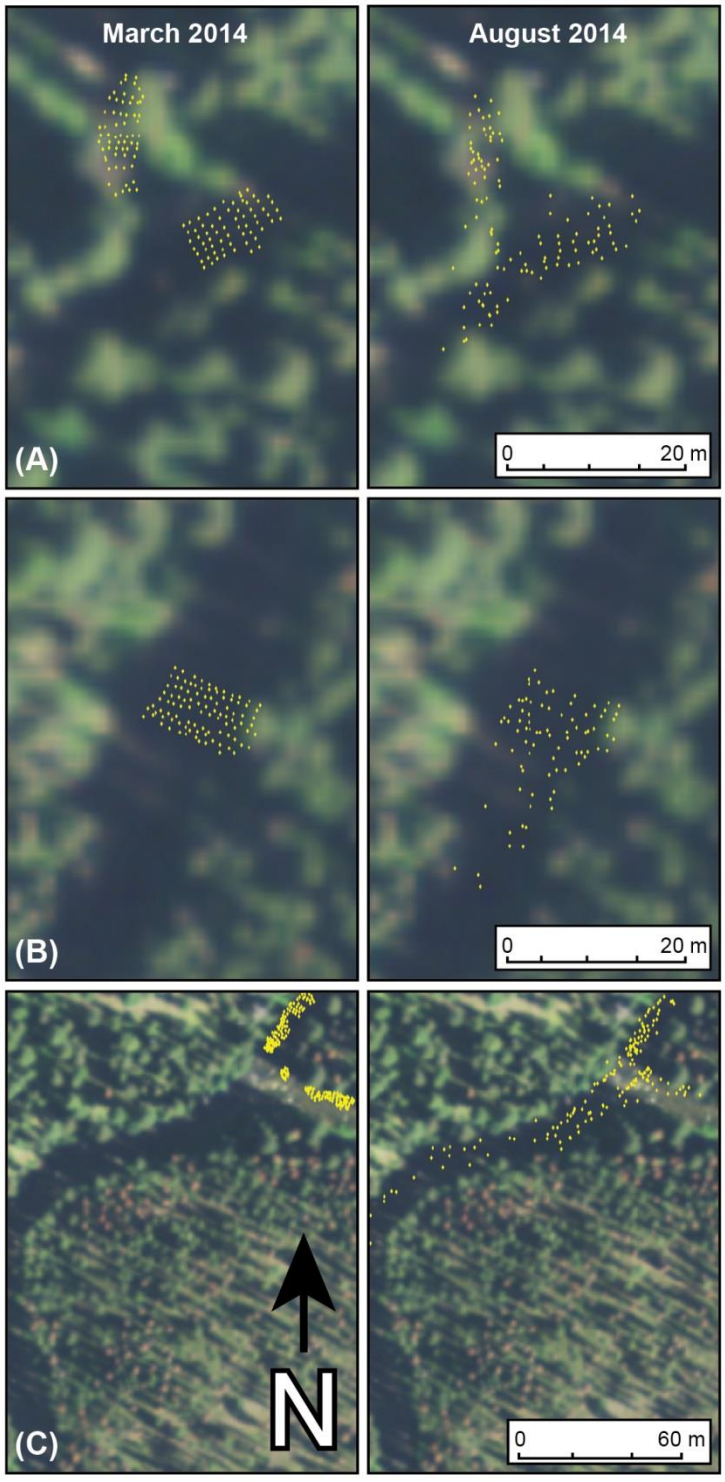

832

833 Figure 5: Tracer positions at initial installation (left) and following the 2014 flood (right) at (A)

834 the upper confluence, (B) control reach, and (C) lower confluence reaches.

835

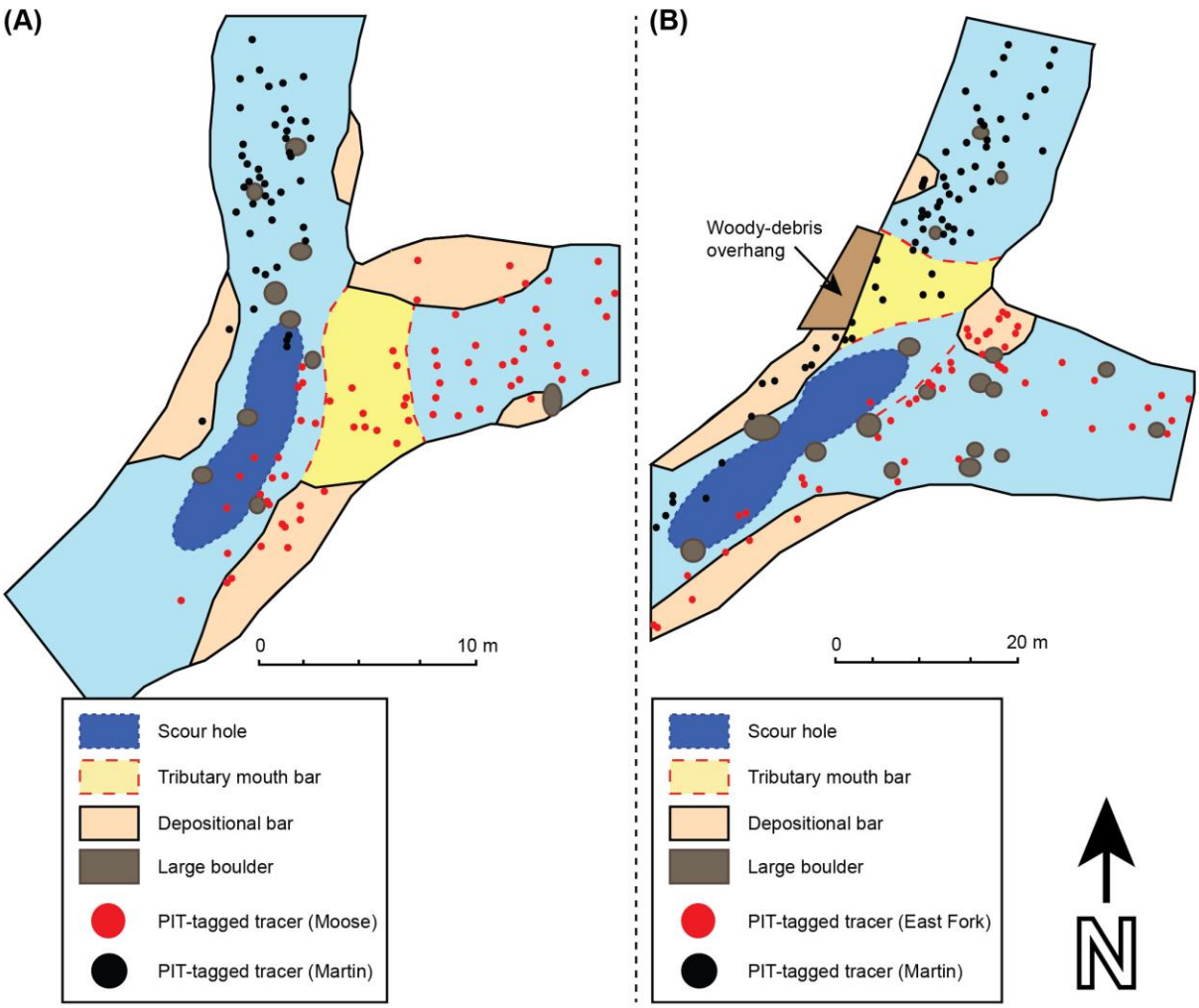

836

837 Figure 6: Digitized patch map of bedforms and tracer recovery positions at the (A) upper and (B)

838 lower confluences.

839

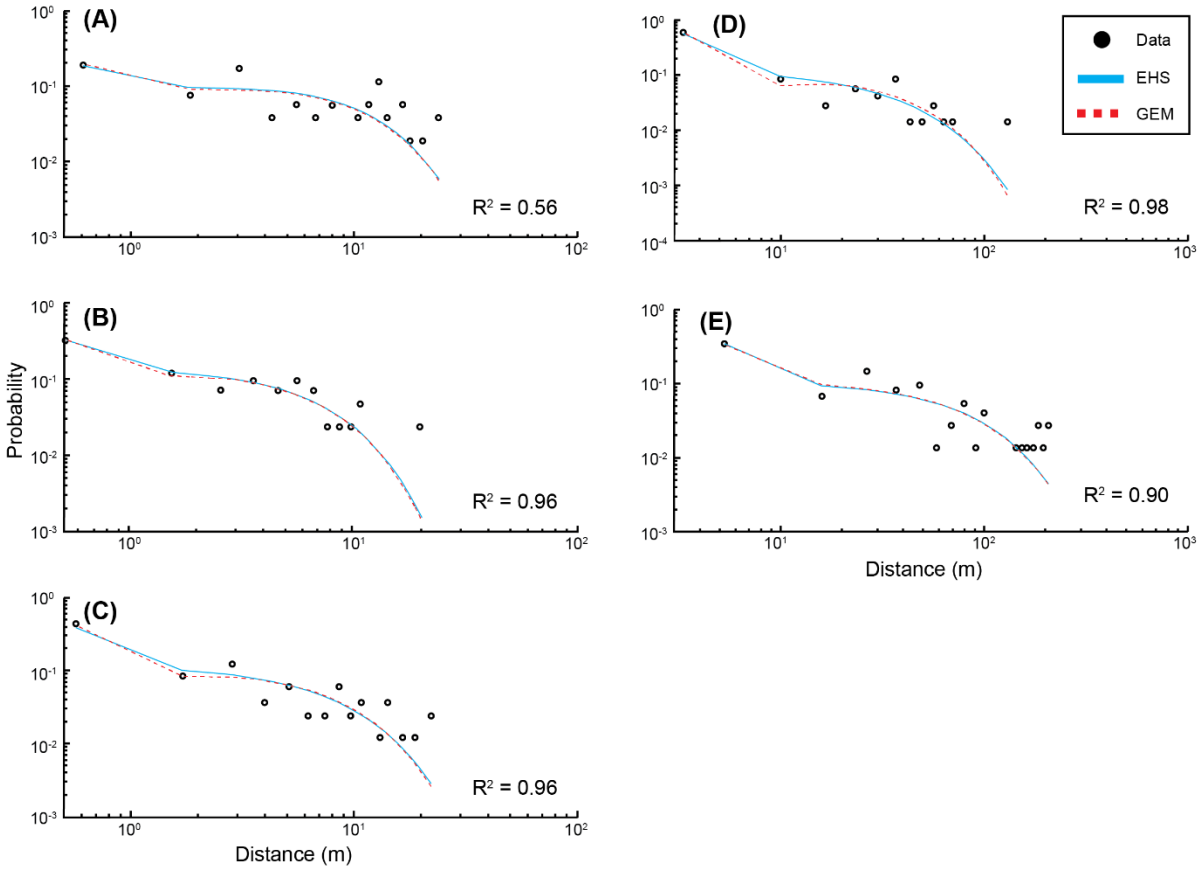

840

841 Figure 7: Einstein-Hubbell-Sayre (EHS) and Yang-Sayre (GEM) model fits for (A) Moose
842 Creek, (B) Martin Creek (upper), (C) the control reach, (D) Martin Creek (lower), and (E) the
843 East Fork Bitterroot River. R^2 fit differences between the two models were < 0.01, so we present
844 their shared fit values here.

845

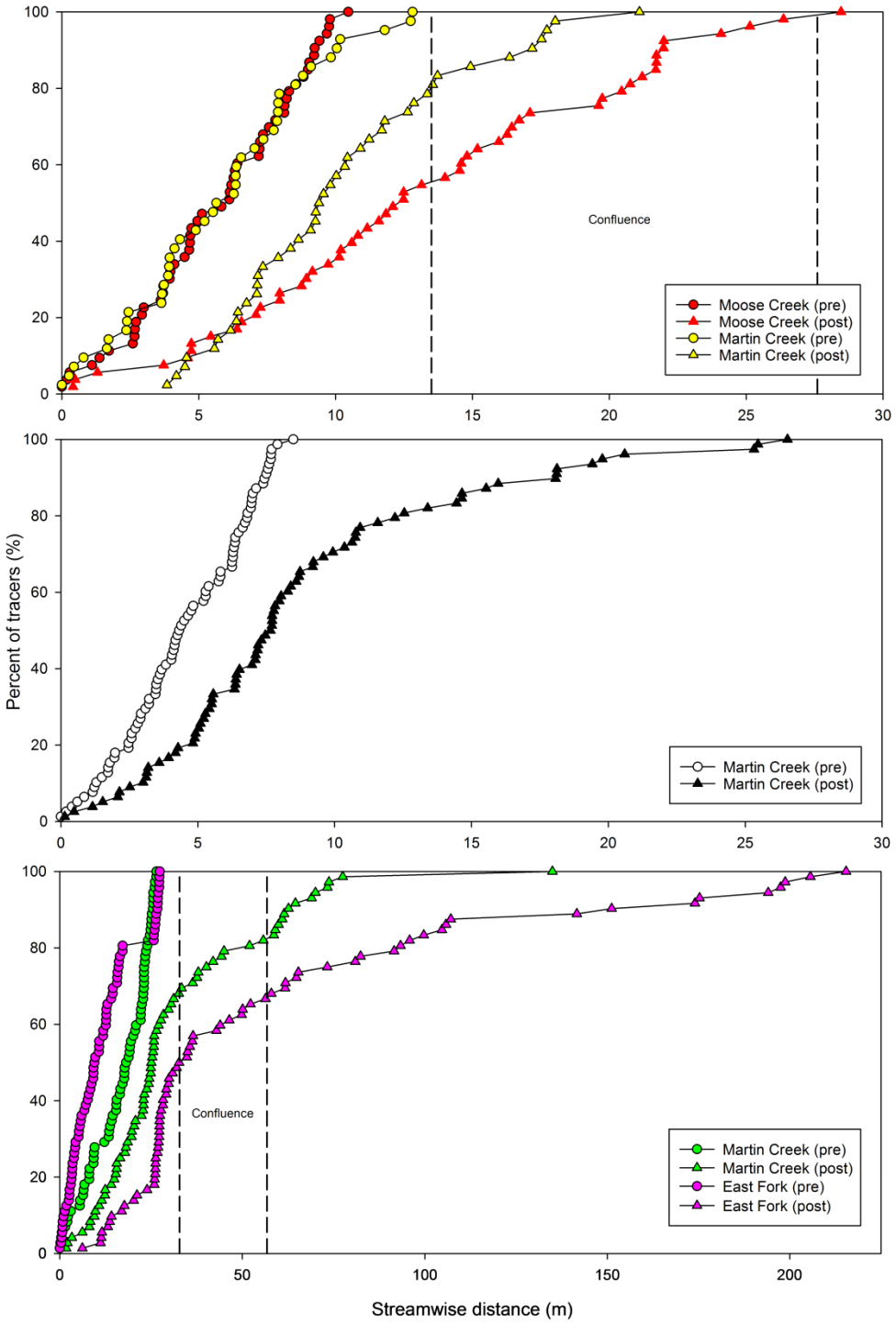

Figure 8: Spatial distribution of tracer positions at the time of initial deployment (pre) and after the 2014 flood (post) for (A) the upper confluence, (B) the control reach, and (C) the lower confluence. The confluence zones are bracketed with dotted vertical lines. Note the altered x-axis scale in (C).

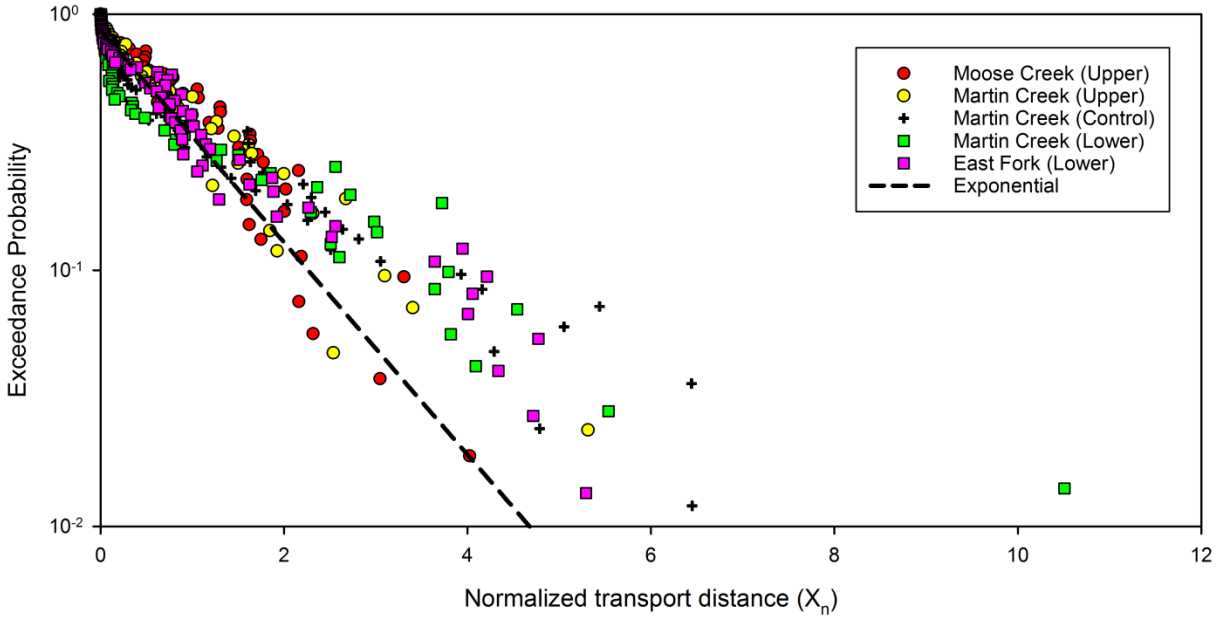

Figure 9: Normalized transport distances (X_n; Eq. 1) in all five study reaches.

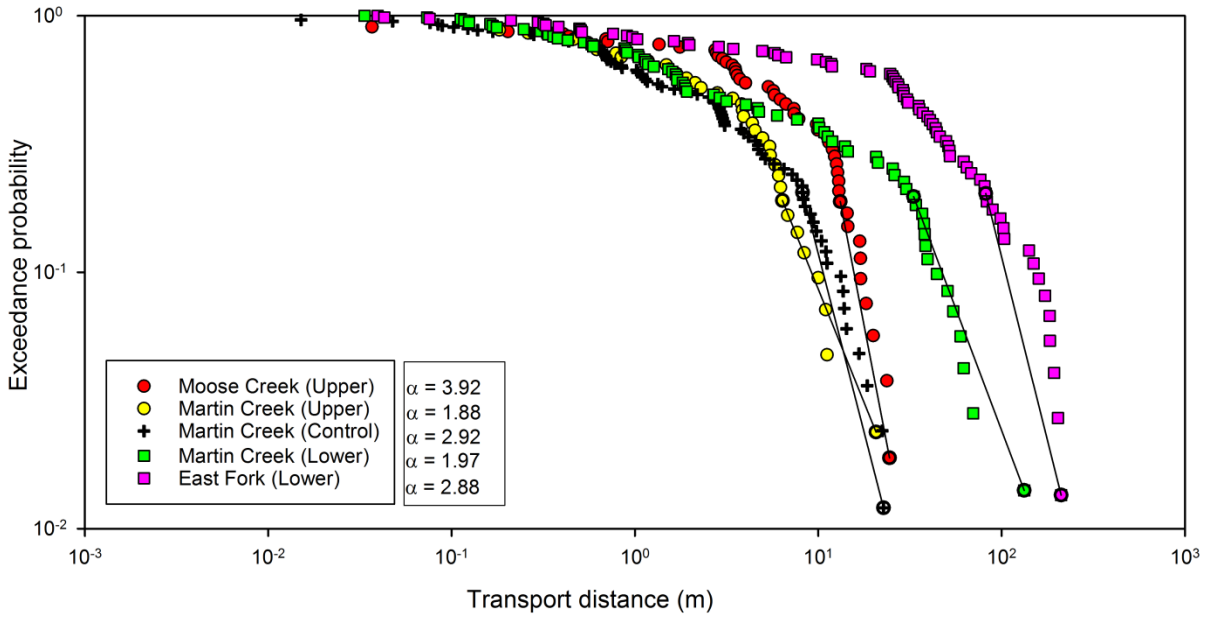

Figure 10: Cumulative exceedance distributions of travel distance for the upper confluence, lower confluence, and control reach.

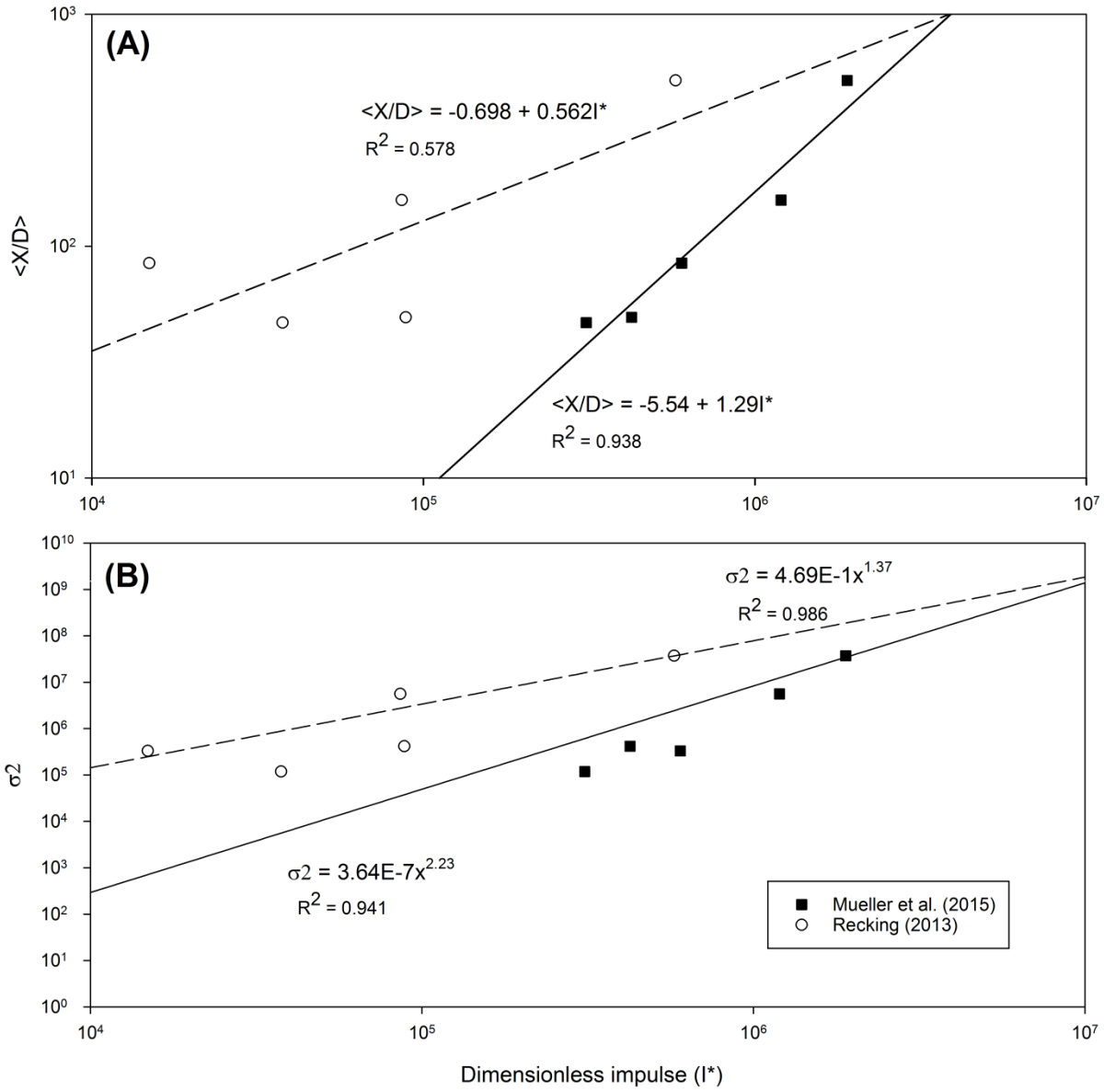

Figure 11: Linear and power-law relations between dimensionless impulse and (A) <X/D> and (B) σ^2.

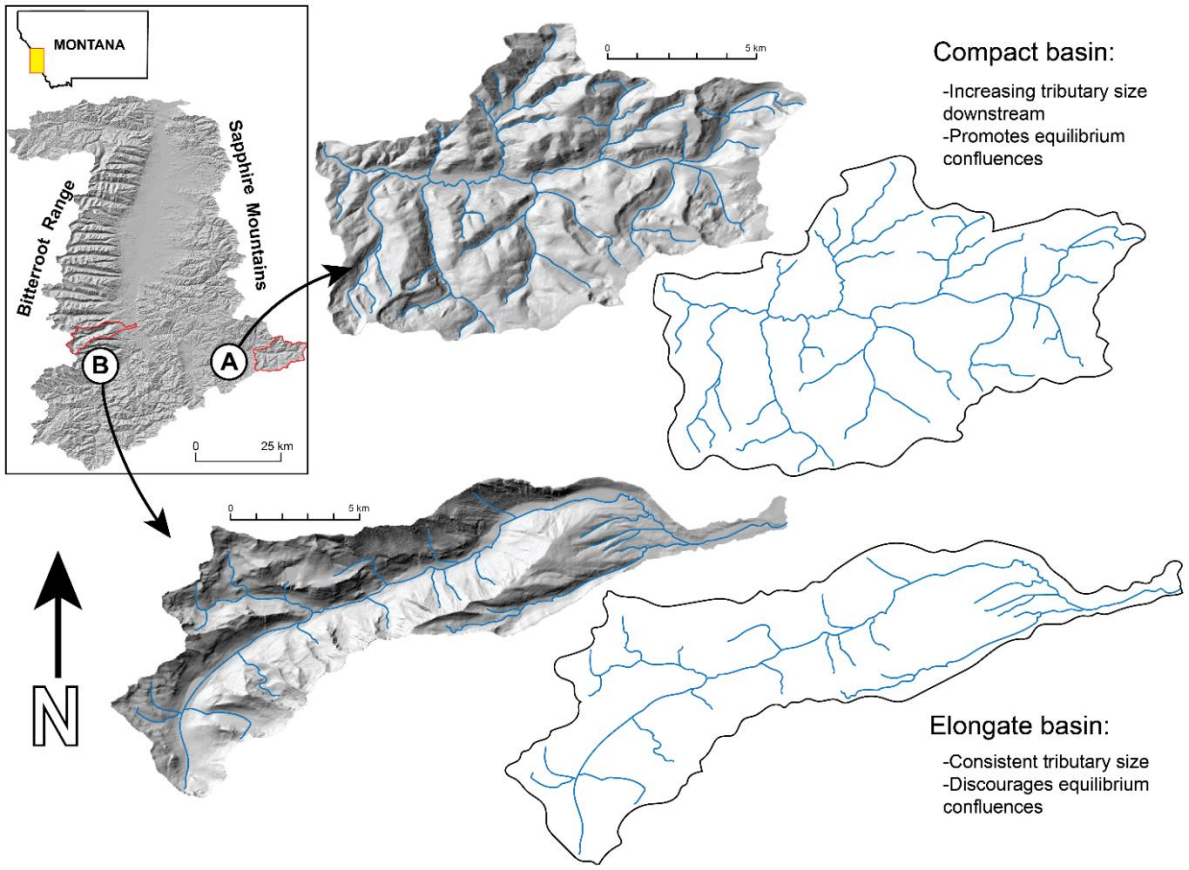

Figure 12: Typical basin shapes and tributary sizes in the (A) Sapphire Mountains (East Fork Bitterroot River) and (B) Bitterroot Range (Tin Cup Creek). These basins are of similar drainage area, but differ in lithology, erosional history, basin morphology, and potential sediment routing.